Article

Not peer-reviewed version

Single CsPbBr3 Perovskite Microcrystals: From Microcubes to Microrods with Improved Crystallinity and Green Emission

Khouloud Abiedh , Marco Salerno * , Fredj Hassen , Zaaboub Zouhour

Posted Date: 24 July 2024

doi: 10.20944/preprints202407.1799.v1

Keywords: perovskite; microrods; aminosilane; optical properties; surface modification

Article

Single $CsPbBr_3$ Perovskite Microcrystals: From Microcubes to Microrods with Improved Crystallinity and Green Emission

Khouloud Abiedh [1], Marco Salerno [2,*], Fredj Hassen [1] and Zouhour Zaaboub [1]

[1] Micro-Optoelectronics and Nanostructures Laboratory (LR99/ES29), Faculty of Sciences, University of Monastir, Monastir 5000, Tunisia; abiedh.khouloud@fsm.u-monastir.tn, fredj.hassen@fsm.u-monastir.tn, zouhour.zaaboub@isimm.rnu.tn

[2] Department of Physics, University of Genoa, via Dodecaneso 33, 16146 Genoa, Italy, and IGDORE; marco.salerno@unige.it

* Correspondence: marco.salerno@unige.it; Tel.: +39-010-3356248

Abstract: All-inorganic perovskite materials are promising in optoelectronics but their morphology is a key parameter for achieving high device efficiency. We prepared $CsPbBr_3$ perovskite microcrystals with different shape, grown directly on planar substrate by conventional drop casting. We observed the formation of $CsPbBr_3$ microcubes on bare indium tin oxide (ITO) coated glass. Interestingly, with the same technique $CsPbBr_3$ microrods were obtained on (3-Aminopropyl) triethoxysilane (APTES) modified ITO-glass, which we ascribe to modification of formation kinetics. The obtained microcrystals exhibit orthorhombic structure. Green photoluminescence (PL) emission is revealed from the $CsPbBr_3$ microrods. Contact angle measurements, Fourier-transform infrared and PL spectroscopies confirmed that APTES linked successfully to the ITO-glass substrate. We propose a qualitative mechanism to explain the anisotropic growth. The microrods exhibited improved PL and slower PL lifetime compared to the microcubes, likely due to diminished occurrence of defects. This work demonstrates the importance of the substrate surface to control the growth of perovskite single crystals and to boost the radiative recombination in view of high performance optoelectronic devices.

Keywords: perovskite; microrods; aminosilane; optical properties; surface modification

1. Introduction

Due to the solution processability [1], low cost [2], high stability [3] and narrow emission line [4], all-inorganic cesium halide perovskites $CsPbX_3$ (X=Cl, Br and I) have recently attracted high interest in optoelectronic applications [4,5]. These members of the perovskite family appear to be a promising alternative to traditional semiconductors, yet require improvement in synthesis and understanding of their properties. Several synthesis protocols have been developed in order to obtain all-inorganic perovskite in different form, such as microcrystals [6], thin films [1,7] and nanocrystals (NCs) [4]. However, most of those strategies do not allow a proper control of shape and size. Synthesis of material with high quality and well-defined morphology not only benefits fundamental research but also offers great promise for practical application [8]. In the arena of NCs, the synthesis protocols based on solution phase such as hot injection [9] or ligand assisted precipitation [10] have shown their potential in regulating the final morphology of the $CsPbBr_3$ NCs, promoting the selective formation of nanocubes, nanoplates and nanowires, by acting on the acid-base equilibrium mechanism [11]. NCs with a variety of shapes have been synthesized by kinetically controlling the growth of particular facets [12] or through an oriented attachment mechanism [13]. The surface chemistry of NCs is decisive in determining the final morphology of the material [14]. Surfactant or surface ligands such as alkylamine and carboxylic acid have been proven essential to alter the kinetic pathways and give anisotropically developed nanostructures, forming hydrogen bonds with

 doi:10.20944/preprints202407.1799.v1

bromide anionic surface sites and alkyl carboxylate binding the surface cationic sites [12]. However, the shape control of single microcrystals is less explored.

In this study, we investigated the effects of the (3-aminopropyl)triethoxysilane (APTES) surface ligand-modified substrate on the growth of $CsPbBr_3$ perovskite single microcrystals. A silane layer is usually employed to control the physical and chemical properties of a solid surface [11]. APTES is a surface ligand extensively employed to functionalize surface with amino silane via covalent interaction [15]. Attachment of primary amine seems an effective technique to control the growth of all inorganic $CsPbBr_3$ perovskite. Our work shows unpreceded method to prepare $CsPbBr_3$ single microcrystals via a solution processing strategy, which gave rise to uniaxial directional growth of elongated crystals that we called microrods (MRs) crystallizing in orthorhombic phase. The presence of functional groups of silane layer and the possible chemical bonding to $CsPbBr_3$ perovskite was confirmed by Fourier-transform infrared spectroscopy (FTIR). The synthesis technique in this study is facile and offers a new procedure to grow $CsPbBr_3$ perovskite MRs structure with improved properties for optoelectronic application.

2. Materials and Methods

2.1. Surface Treatment

If not otherwise specified, all chemicals and materials were acquired from Sigma-Aldrich. ITO-coated glass wafers to be used as the substrates were rinsed sequentially with absolute ethanol and acetone in a bath ultra-sonicator. The cleaned wafers were hydroxylated via Piranha treatment at room temperature (RT) for 20 min and with an H_2O_2/H_2SO_4 (3:7) at 60 °C, and then rinsed with water and dried with argon flux. For silanization process the substrates were immersed in 2% toluene solution during 3 min. Finally, the substrates were rinsed with toluene and deionized water and then dried in a nitrogen stream.

2.2. Perovskite Preparation

We prepared $CsPbBr_3$ precursor solution by mixing CsBr and $PbBr_2$ in dimethyl sulfoxide (DMSO). The solution of precursor was magnetically stirred before deposition. The precursor solution was deposited on silane-functionalized surface by drop casting. After the deposition onto the substrate, a short annealing was conducted.

2.3. Characterization

X-ray diffraction (XRD) patterns were obtained using a PAN analytical Empyrean X-ray diffractometers equipped with 1.8 Kw CuKα ceramic X-ray tube and operating at 45 kV and 40 mA.

Optical microscopy images and 3D profilometry measurements were obtained with a confocal Zeta-20 profilometer (Zeta instruments, USA).

Atomic force microscopy (AFM) measurements were performed with a XE 100 (Park Systems, Korea) microscope under ambient atmosphere.

PL microscopy was used to obtain images and to acquire spectrum of individual microcrystals under 488 nm wavelength (blue light) excitation, with collection in the cyan-green window (500–550 nm).

UV-Visible absorbance spectra were measured using a SPECORD 210-PLUS spectrophotometer, equipped with a deuterium D2E lamp (185 nm-350 nm), and a halogen lamp (330 nm-1100 nm).

Steady state PL spectra were measured at 300 K using laser excitation wavelength of 360 nm. Spectral analysis of the luminescence measurements was dispersed using JOBIN YVON HRDI (iHR320) monochromator and detected by a silicon photodiode.

Time resolved PL (TRPL) measurements of the recombination dynamics were carried out by time correlated single photon counting setup based on the pulsed laser diode ($\lambda_{ex} = 375\,nm$) operated at 80 MHz and time Harp 200 electronic card from Pico Quant company16. The excitation laser pulse width was 70 ps, the time resolution of the experimental setup was 40 ps. The lifetimes t

 doi:10.20944/preprints202407.1799.v1

were obtained by fitting the experimental data of PL intensity I_{PL}, as compared to initial intensity I_0, to a mono-exponential decay:

$$I_{PL}(t) = I_0\, e^{\frac{-t}{\tau}} \quad (1)$$

Contact angle (CA) measurements were carried out by the CA goniometer Digidrop GBX, using the Laplace- Young method [17].

FTIR spectra were recorded using Perkin Elmer spectrometer equipped with a universal attenuated total reflectance mode and scanned at RT in transmission mode over the wave number range of 4000-850 cm^{-1}.

3. Results and Discussion

$CsPbBr_3$ microcrystals were prepared on solid substrates in two forms: the novel MRs (elongated in one planar direction) and the planar-symmetric microcrystals already presented in previous works [18,19], which we call here microcubes (MCs). Actually, the name MCs is to simplify the description, as the microcrystals are anyway not full cubes, yet have a hollow pyramidal pit on top, discussed extensively in our previous reports [18,19]. The MCs will be used here as a term of comparison for the novel MRs structures. A morphological characterization of the MCs is reported in Figure 1a–c. An optical micrograph of the sample (Figure 1a) shows the presence of squares shaped structures (see also the 3D optical profilometer image of the same region in Figure 1b). The MCs are quite homogenous in size (see distribution in Figure 1c), with an edge length of ~64 μm. The preparation parameters are critical for the final microstructure size. The XRD pattern (Figure 1g) evidences the crystalline nature of the MCs, which matches the orthorhombic perovskite phase. The UV-visible absorption spectrum of the as-prepared sample presented in Figure 1i shows the typical profile of $CsPbBr_3$ microcrystals, characterized by an absorption peak at ~517 nm. The PL spectrum of the MCs shows a narrow and intense band (fullwidth at half maximum ~17 nm) centered at ~519 nm (2.39 eV). The emission band is associated to the bulk bandgap recombination of $CsPbBr_3$ [19].

Figure 1d,e present some perovskite MRs deposited on APTES-modified ITO-glass substrate. The images show the formation of well-defined rectangular single rods. Obviously the effect of the APTES modified substratewas the transformation of crystals from MCs to MRs. In the given fabrication conditions, the aspect ratio of the MRs (ratio of long side to short side) is ~5, while the longest diagonal is ~200 μm. The size distribution histogram for the latter parameter is presented in Figure 1f. According to the histogram, the spread around the peak size value is described by a standard deviation of ~30 μm. For the off-plane size of the MRs, optical profilometer measurements (see a representative 3D image in Figure 1d) showed a MRs thickness in the range of 10 to 25 μm.

The bulk crystallinity of the MRs was confirmed by XRD measurements (see Figure 1h). The majority of peaks, green dots in the diffractogram, fits well with $CsPbBr_3$ orthorhombic perovskite phase (PDF#45-0752, standard diffraction pattern), confirming the formation of $CsPbBr_3$ crystals. The sharp peaks indicate high crystallinity of the MRs. The XRD pattern revealed also the presence of other phases such as Pb (cubic, F m-3 m), and BrN (tetragonal, P 4/n m m).

 doi:10.20944/preprints202407.1799.v1

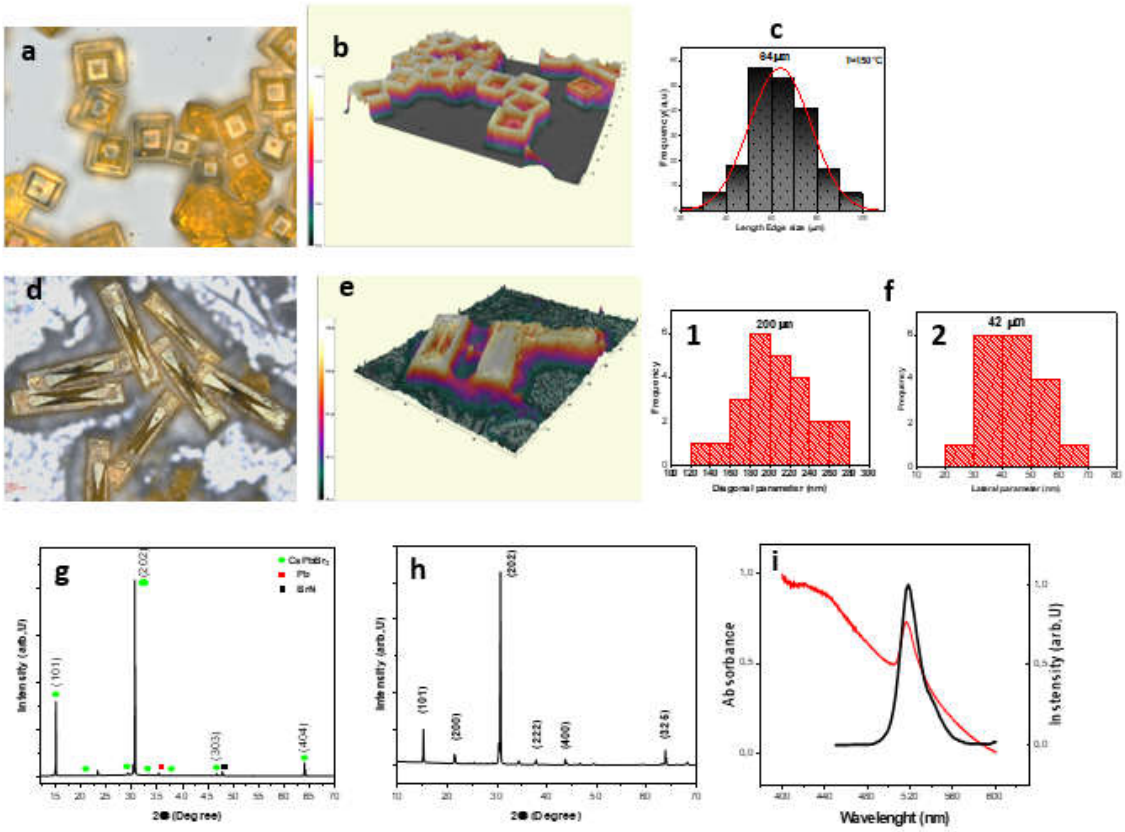

Figure 1. Structural characterization of $CsPbBr_3$ microcrystals. (a) Optical micrograph (scale bar 28 µm) and (b) 3D optical micrograph image of some MCs. (c) Histogram of the edge size parameter of MCs. (d) Optical micrograph (scale bar 28 µm) and (e) 3D optical micrograph image of some MRs. (f) Histogram of the in-plane size diagonal length (1) and (2) lateral size. (g-h) Typical XRD pattern of a MC and MR, respectively. (i) UV-visible absorption and PL spectra of an ensemble of MCs.

High resolution confocal microscopy images (2D and 3D) of the novel MRs have been acquired (Figure 2a,b). Clearly, one can see that the MRs fluoresce in the green region of the visible electromagnetic spectrum. Two PL spectra extracted from different regions of the rods in the confocal image (red and green circles in Figure 2b) are presented in Figure 2c. It appears that the edge of the MR yields a higher PL as compared to the center, and a peak shift towards the red (~530 nm vs ~520 nm). This effect has been confirmed by testing several different MRs. We should point out that our MRs present hollow top with inverted pyramid shape similar to the MCs (see Figure 1b,e). We have shown previously by using PL microscopy that in single $CsPbBr_3$ MCs [18] the emission from the upper surface (near the edge) is different compared to that one from the center. So, The PL intensity change by changing the excitation surface position for single $CsPbBr_3$ microcrystal.

For a deeper understanding of the optical properties of the MRs, a more advanced optical characterization has been carried out. In Figure 2d,e typical absorbance and steady state PL spectrum of the MRs recorded at 300 K are presented, respectively. As we can see, the PL spectrum revealed the presence of two peaks. One peak, named P_1, is located at 442 nm and can be assigned to APTES emission [20], in accordance with the presence of APTES absorption edge feature at 320 nm (inset in Figure 2d). The important emission peak that presents an asymmetrical profile with extended shoulder on the long wavelength side was fitted by two Gaussians with maxima located at 523 and 540 nm, which were denoted P_2 and P_3, respectively. This feature can be attributed to the PL from the $CsPbBr_3$ MRs. Correspondingly, a strong absorbance band at ~520 nm is shown in Figure 2d, which is a characteristic peak of bulk $CsPbBr_3$ perovskite [21]. Figure 2f displays normalized TRPL emission profiles recorded for the sample at RT, at different energies of the emission peaks. It can be seen that profile of P_1 decays faster than that of P_2. The PL decays presented the following lifetimes: t_1~1.62

 doi:10.20944/preprints202407.1799.v1

ns, t_2~4.12 ns and t_3~7.86 ns, for peaks P_1, P_2 and P_3, respectively. Obviously, the longer carrier lifetime results from the delayed recombination process via non-radiative pathways, which means that the P_3 PL peak can be assigned to the emission of shallow defects in the $CsPbrBr_3$ material [21].

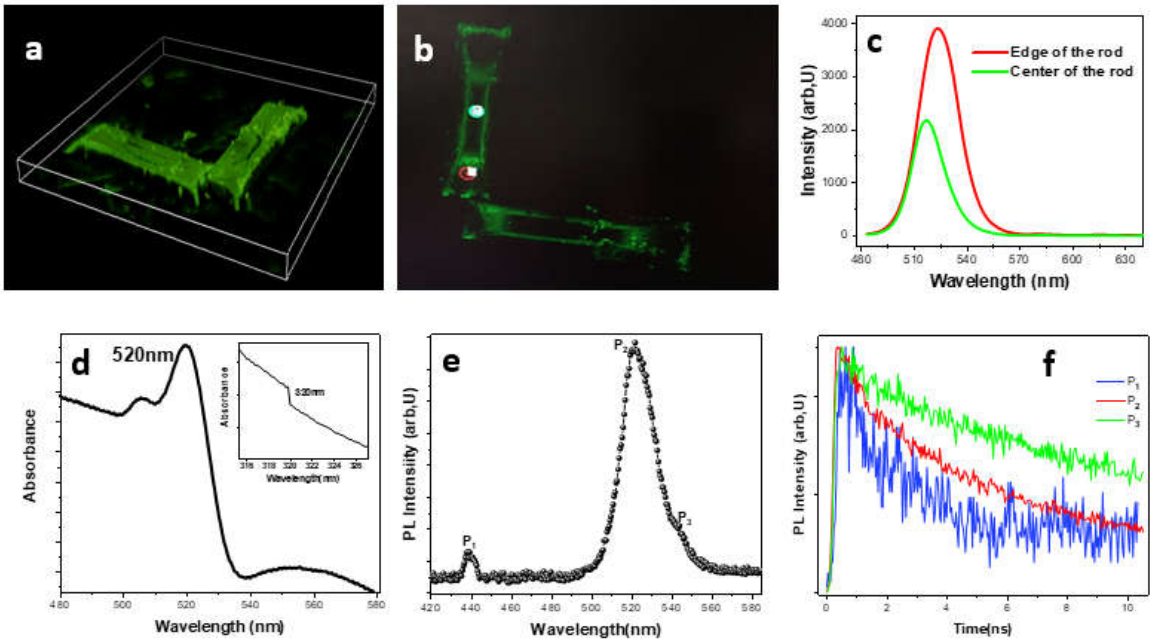

Figure 2. Optical measurements of the MRs. (a) 3D rendering and (b) top-view confocal microscopy image of two MRs. (c) PL spectra obtained from one MR at the spots marked in (b). (d) Absorbance spectrum, (e) steady state PL spectrum and (f) TRPL decay profiles.

CA measurements were carried out to determine the wettability of substrates before and after APTES modification, which are shown in Figure 3a. The obtained CA value for bare ITO-glass was found to be ~39° (Figure 3a1). A significant increase in CA, ~64° (Figure 3a2) was observed for the APTES modified surface (Figure 3b,c). Thus, the surface becomes less hydrophilic on coating with APTES, due to the presence of hydrophobic alkyl chains of this molecule [22,23] (see Figure 3b). The APTES is anchoring the ITO-glass surface by replacing the terminating OH groups of the substrate with organic groups attached to amine groups (see Figure 3c), which changes the surface energy and thus its wettability.

Typically, the silanization process consists of two steps: hydrolysis and condensation. In the first step, hydrolysis of the substrate leads to the formation of the reactive silanol group (R-Si-OH) and ethanol molecules [22]. In the second step, condensation of these silanol groups takes place leading to the formation of siloxane (Si-O-Si) linkages over the surface [22,23]. Thus, attachment of APTES takes place with OH groups on the substrate, and a NH_2 terminated layer is created on the surface (Figure 3c). These amino (-NH_2) groups on APTES surface react with perovskite via chemical bonding. According to literature [24,25], attachment of APTES to $CsPbBr_3$ perovskite takes place through three possible binding mechanisms [15]: (1) formation of dative-covalent bond between amines (NH_2) of silanes network and undercoordinated Pb^{2+} sites; (2) hydrogen bond formation between remaining silanol and surface bromide (Br^-) sites; (3) formation of hydrogen bonds through protonated amines (NH^+) and bromine (Br^-) dangling bonds.

Preprints.org (www.preprints.org) | NOT PEER-REVIEWED | Posted: 24 July 2024 doi:10.20944/preprints202407.1799.v1

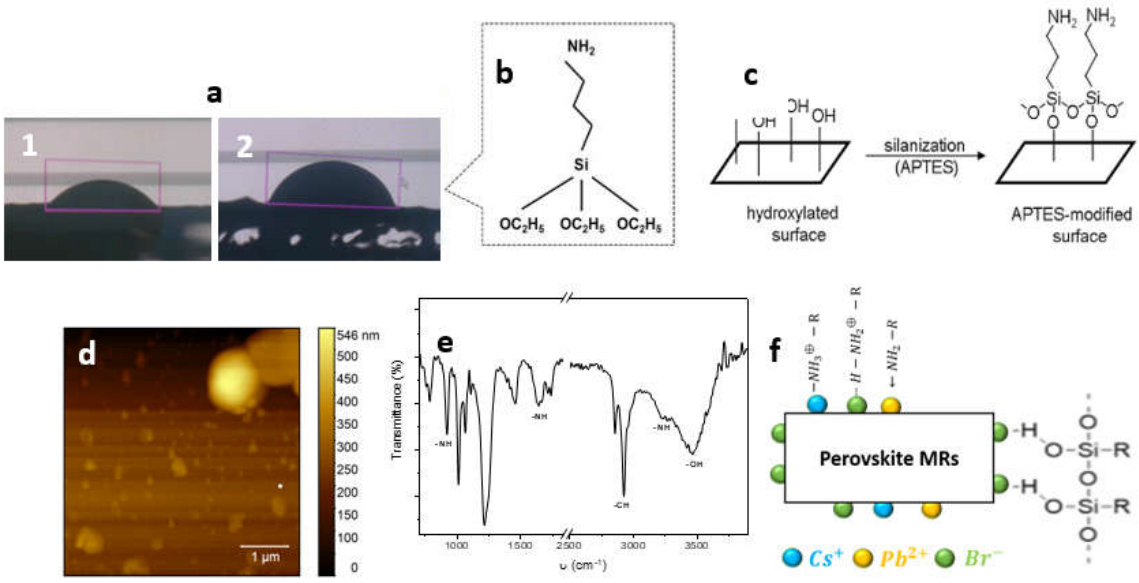

Figure 3. (a) CA measurements of (1) ITO coated glass and (2) APTES/ITO-glass. (b) APTES chemical structure. (c) Silanization process of ITO patterned glass substrate. (d) AFM image of APTES modified-ITO glass substrate. (e) FTIR spectrum of $CsPbBr_3$ MRs deposited on APTES ITO-coated glass substrate. (f) The schematic structure of the possible binding of the obtained rods with aminosilane layers.

For ideal silanization, all amino group of the APTES should be oriented away from the substrate surface [26]. The typical APTES surface quality was as shown in the representative image in Figure 3d, showing a flat and smooth background with some aggregates up to ~1 mm size, likely due to excess material. In fact, the thickness of the APTES layer was also estimated, by using AFM across hand-made scratches in the molecular coating, which resulted in a value around ~150 nm (data not shown). The thickness of one silane layer is ~2 nm [27], which confirms the formation of multisilane layers on the top of ITO-glass substrate.

The surface chemical composition of $CsPbBr_3$ MRs was characterized by FTIR measurements (see Figure 3e). The resulting peaks assignment is reported in Table 1. FTIR results confirm the presence of asymmetric stretching vibration of surface hydroxyl groups (OH) by the broad band at 3464 cm^{-1}, due to ethanol. This large band shows a small peak located at 3258 cm^{-1}, due to the N-H symmetric stretching vibration of APTES [28]. Bands at 2856 cm^{-1}, 2925 cm^{-1} and 2959 cm^{-1} corresponds to C-H vibration from both ethanol and APTES [28]. Bands at 1638-1664 cm^{-1} are attributed to binding vibration of primary amines (NH_2) in APTES [28]. The appearance of these bands demonstrated that amine functional groups in organosilane were successfully grafted onto the ITO-glass substrate [28].

Furthermore, peaks corresponding to Si-O-Si bond were observed at around 1012 cm^{-1}-1066 cm^{-1}, indicating the condensation reaction between silanol groups [28]. These bands confirm condensation reaction between ethoxy groups of APTES and the ITO surface hydroxyl groups, namely ITO-glass modification with APTES. The FTIR spectrum shows another weak peak at 1575 cm^{-1}, which was assigned to the NH^+ bond [9]. In conclusion, FTIR spectroscopy confirms the presence of characteristic functions of APTES on the sample surface and the attachment of perovskite to the APTES through three different binding due to the presence of NH_2, NH^+ and silanol groups on the surface of the rods (see Figure 3f).

Table 1. FTIR bands and peak assignments.

Wavenumber (cm^{-1})	Functional group
3464	-OH
3258	-NH

 doi:10.20944/preprints202407.1799.v1

2959-2924-2856	-CH
1715-1734	-CH
1638-1664	$-NH_2$
1453	C-H
1244-1213	C-H
1012-1066	Si-O-Si
922	CH_3 rocking of APTES
755-788	Ethoxy group of APTES

To figure out the origin of anisotropic growth of $CsPbBr_3$ MRs, we propose a plausible mechanism. In precursor solution, the Br^- ions coordinate with Pb^{2+} to form $[PbBr_6]^{4-}$ octahedra in DMSO. After precursor solution deposition, the solvent is evaporated under heat treatment to allow crystallization of perovskite [29], and the Cs^+ ions occupy the octahedral sites to form $CsPbBr_3$ perovskite MCs above bare ITO-glass substrate. This occurs by using the same precursor solution for both MRs and MCs, which means that MRs evolve from MCs during heating process. The crystallization process (nucleation and growth) plays an important role in determining the crystal structure, shape and size [30]. According to literature, nano/micro or macro crystals synthesis with various size and shapes can described via supersaturation chemistry approach (Lamer theory) [30,31]. Shape control of $CsPbX_3$ perovskite NCs has been tuned either by kinetically controlling the growth of particular crystal facets [12] or through an oriented attachment mechanism [13]. In contrast, few studies deal with anisotropic microparticles formation mechanism. Consequently, a hypothetical approach to understand the mechanism of microcrystals construction provides a greater control over the size, shape and structure of single crystals and consequent the ability to tune the properties by varying the crystallization conditions.

The growth rate of the single crystal increases with the increase of CA. The less hydrophilic APTES-modified surface makes precursor ions and solvent to get closer, which will increase the diffusions of ions, leading to a faster crystal growth. In fact, it is known that, at high growth rates, organic molecules (ligands) that selectively adhere to particular NC facets decrease their energy and slow down their growth [32]. High-energy facets grow faster than low-energy ones, giving rise to the formation of anisotropic shape [33]. Previously, Pan et al. [9] suggested preferential binding of amine toward certain facets during the growth of $CsPbBr_3$ nanowires and nanoplatelets. Also, it is demonstrated that ammonium binding with Cs^+ ions on the surfaces allows the growth of platelets [33]. So, we suppose here that the amine groups compete with the Cs^+ ions on the surface of the growing rods, and thus it slows the growth along the orthogonal direction, leading to the observed anisotropic rod structures. Also, it is suggested that halide-rich environment may result in oriented crystal growth along special facets.

In support of our hypothesis that preferential binding of APTES takes place through amine groups giving rise to the formation of perovskite MRs, we have compared the PL properties of MCs and MRs. The PL spectrum of MRs is slightly redshifted with respect to MCs ones (see Figure 4). The PL maximum slightly redshifts from the 519 nm for MCs to 523 nm for MRs. MRs also show PL enhancement compared to MCs. The origin of enhancement may arise from the effective surface passivation by APTES molecules. TRPL spectra of the microcrystals were also acquired and fitted using a biexponential decay function where A_i and τ_i refer to the decay amplitudes and respective PL lifetimes, for i=1,2. The average lifetime can thus be obtained by the following formula:

$$\tau_{av} = A_1\tau_1 + A_2\tau_2 \quad (2)$$

 doi:10.20944/preprints202407.1799.v1

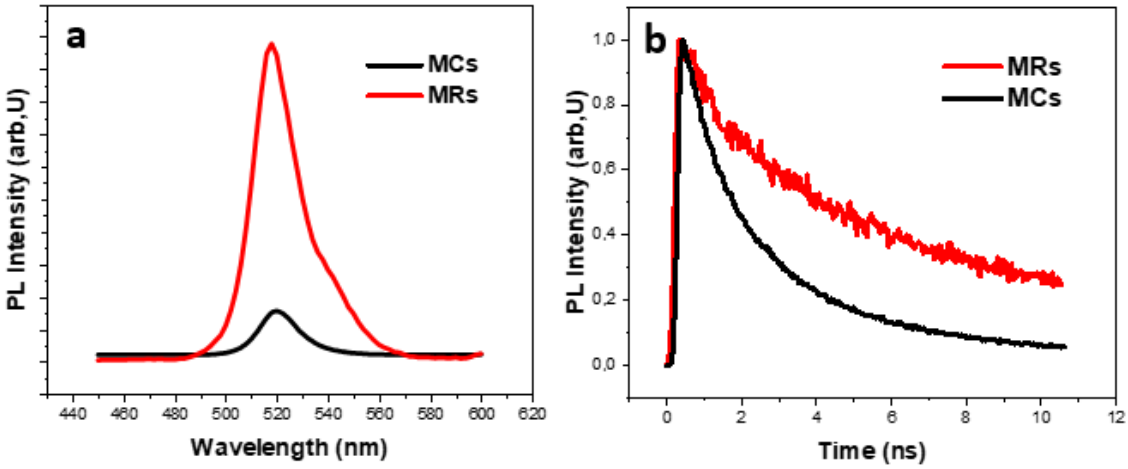

Figure 4. (a) CA measurements of (1) ITO coated glass and (2) APTES/ITO-glass. (b) APTES chemical structure. (c) Silanization process of ITO patterned glass substrate. (d) AFM image of APTES modified-ITO glass substrate. (e) FTIR spectrum of $CsPbBr_3$ MRs deposited on APTES ITO-coated glass substrate. (f) The schematic structure of the possible binding of the obtained rods with aminosilane layers.

The time-resolved measurements also show an enhancement of the PL lifetime upon APTES treatment (see Figure 4b), from ~2.3 to ~7.4 ns). This behavior may arise from enhanced passivation of the $CsPbBr_3$ MRs surfaces.

Table 2. PL lifetimes of $CsPbBr_3$ MCs and MRs.

sample	A_1	τ_1(ns)	A_2	τ_2(ns)	τ_{Av}(ns)
MCs	54.65	3,39	45.35	1.01	2.31
MRs	72.56	9.95	19.79	1.10	7.43

4. Conclusions

In summary, we presented a comparative study of $CsPbBr_3$ perovskite microcrystals with different form, grown directly on planar substrate by conventional drop casting method. We observed the formation of $CsPbBr_3$ MCs on bare ITO-coated glass substrate. With the same technique, $CsPbBr_3$ single MRs were obtained on APTES surface ligand modified ITO-glass substrate, which we ascribed to the modification of the kinetic regime by using APTES. Green emission was revealed from the $CsPbBr_3$ microcrystals by using PL spectroscopy. CA measurements, FTIR and PL spectroscopies confirmed that APTES linked successfully to ITO-coated glass substrate. The fabricated perovskite MRs exhibited improved PL thanks to the introduced APTES molecules effectively passivating surface defects and controlling the crystal growth. We conclude that, even for microcrystals, introduction of certain organic molecules that selectively adhere to a particular crystal facet can be used to slow the growth of that side relative to others, leading to the formation of various shapes singles crystals. Thus, we have identified a new strategy to enhance the photoluminescence and to control the shape of $CsPbBr_3$ microcrystals for optoelectronic application. Further research work is needed to confirm these findings, still our work points out that careful management of the perovskite MCs and substrate surface engineering are important factors in this promising class of optoelectronic materials.

Author Contributions: Conceptualization and methodology, K.A. and Z.Z.; formal analysis, K.A: and F.H.; investigation, K.A. and M.S.; resources, F.H. and Z.Z.; data curation, K.A.; writing—original draft preparation, K.A.; writing—review and editing, M.S., F.H. and Z.Z.; visualization, K.A.; supervision and funding acquisition, F.H. and Z.Z.. All authors have read and agreed to the published version of the manuscript.

Funding: This research received no external funding.

Institutional Review Board Statement: Not applicable.

Informed Consent Statement: Not applicable.
Data Availability Statement: Data available on request to K.A.

Acknowledgments: KA wishes to thank Dr. Roman Krahne of the Italian institute of technology (iit) for the confocal microscope measurements.

Conflicts of Interest: The authors declare no conflicts of interest.

References

1. Li, Y.; Shi, Z.F.; Li, S.; Lei, L.Z.; Ji, H.F.; Wu, D.; Xu, T.T.; Tian, Y.T.; Li, X.J. High-performance perovskite photodetectors based on solution-processed all-inorganic $CsPbBr_3$ thin films. *J. Mater. Chem. C* 2017, *5*, 8355–8360.
2. Cui, J.; Xu, F.; Dong, Q.; Jia, J.; Liu, L.; Liu, S.; Yang, F.; Ye, X. Facile, low-cost, and large-scale synthesis of $CsPbBr_3$ nanorods at room-temperature with 86% photoluminescence quantum yield. *Mater. Res. Bull.* 2020, *124*, 110731.
3. Zhou, Y.; Zhao, Y. Chemical stability and instability of inorganic halide perovskites. *En. & Envir. Sci.* 2019, *12*, 1495-1511.
4. Protesescu, L.; Yakunin, S.; Bodnarchuk, M.I.; Krieg, F.; Caputo, R.; Hendon, C.H.; Yang, R.X.; Walsh, A.; Kovalenko, M.V. Nanocrystals of Cesium Lead Halide Perovskites ($CsPbX_3$, X=Cl, Br, and I): Novel Optoelectronic Materials Showing Bright Emission with Wide Color Gamut. *Nano Lett.* 2015, *15*, 3692–3696.
5. Liu, X.; Wang, Y.; Wang, Y.; Zhao, Y.; Yu, J.; Shan, X.; Tong, Y.; Lian, X. Recent advances in perovskites-based optoelectronics. *Nanotech. Rev.* 2022, *11*, 3063–3094.
6. Zhang, H.; Liu, X.; Dong, J.; Yu, H.; Zhou, C.; Zhang, B.; Xu, Y.; Jie, W. Centimeter-Sized Inorganic Lead Halide Perovskite $CsPbBr_3$ Crystals Grown by an Improved Solution Method. *Cryst. Growth Des.* 2017, *17*, 6426–6431.
7. Yu, J.; Liu, G.; Chen, C.; Li, Y.; Xu, M.; Wang, T.; Zhao, G.; Zhang, L. Perovskite $CsPbBr_3$ crystals: growth and applications. *J. Mater. Chem. C* 2020, *8*, 6326–6341.
8. Ding, J.; Du, S.; Zuo, Z.; Zhao, Y.; Cui, H.; Zhan, X. High Detectivity and Rapid Response in Perovskite $CsPbBr_3$ Single-Crystal Photodetector. *J. Phys. Chem. C* 2017, *121*, 4917–4923.
9. Pan, A.; He, B.; Fan, X.; Liu, Z.; Urban, J.J.; Alivisatos, A.P.; He, L.; Liu, Y. Insight into the Ligand-Mediated Synthesis of Colloidal $CsPbBr_3$ Perovskite Nanocrystals: The Role of Organic Acid, Base, and Cesium Precursors. *ACS Nano* 2016, *10*, 7943–7954.
10. Mu, Y.; He, Z.; Wang, K.; Pi, X.; Zhou, S. Recent progress and future prospects on halide perovskite nanocrystals for optoelectronics and beyond. *iScience* 2022, *25*, 105371.
11. Zhu, M.; Li, C.; Li, B.; Zhang, J.; Sun, Y.; Guo, W.; Zhou, Z.; Pang, S.; Yan, Y. Interaction engineering in organic–inorganic hybrid perovskite solar cells. *Mater. Horizons* 2020, *7*, 2208–2236.
12. Bealing, C.R.; Baumgardner, W.J.; Choi, J.J.; Hanrath, T.; Hennig, R.G. Predicting Nanocrystal Shape through Consideration of Surface-Ligand Interactions. *ACS Nano* 2012, *6*, 2118–2127.
13. Cho, K.; Talapin, D.V.; Gaschler, W.; Murray, C.B. Designing PbSe nanowires and nanorings through oriented attachment of nanoparticles. *JACS* 2005, *19*, 7140–7147.
14. Fanizza, E.; Cascella, F.; Altamura, D.; Giannini, C.; Panniello, A.; Triggiani, L.; Panzarea, F.; Depalo, N.; Grisorio, R.; Suranna, G.P.; Agostiano, A.; Curri, M.L.; Striccoli, M. Post-synthesis phase and shape evolution of $CsPbBr_3$ colloidal nanocrystals: The role of ligands. *Nano Research* 2019, *12*, 1155-1166.
15. Wen, X.; Wu, J.; Gao, D.; Lin, C. Interfacial engineering with amino-functionalized graphene for efficient perovskite solar cells. *J. Mater. Chem. A* 2016, *4*, 13482–13487.
16. Abiedh, K.; Zaaboub, Z.; Hassen, F. Mixed monomolecular and bimolecular-like recombination processes in $CsPbBr_3$ perovskite film revealed by time-resolved photoluminescence spectroscopy. *Appl. Phys. A* 2021, *127*, 1–9.
17. Boutar, Y.; Naïmi, S.; Mezlini, S.; Da Silva, L.F.M.; Hamdaoui, M.; Ben Sik Ali, M. Effect of adhesive thickness and surface roughness on the shear strength of aluminium one-component polyurethane adhesive singlelap joints for automotive applications. *J. Adhes. Sci. Technol.* 2016, *30*, 1913–1929.
18. Abiedh, K.; Dhanabalan, B.; Kutkan, S.; Lauciello, S.; Pasquale, L.; Toma, A.; Salerno, M.; Arciniegas, M.P.; Hassen, F.; Krahne, R. Surface-Dependent Properties and Tunable Photodetection of $CsPbBr_3$ Microcrystals Grown on Functional Substrates. *Adv. Opt. Mater.* 2021, *10*, 2101807.
19. Khouloud, A.; Hassen, F.; Zaaboub, Z.; Salerno, M. Evaluating the optoelectronic properties of individual $CsPbBr_3$ microcrystals by electric AFM techniques. *Curr. Appl. Phys.* 2024, *62*, 1–6.
20. Gammoudi, H.; Belkhiria, F.; Sahlaoui, K.; Zaghdoudi, W.; Daoudi, M.; Helali, S.; Morote, F.; Saadaoui, H.; Amlouk, M.; Jonusauskas, G.; Cohen-Bouhacina, T.; Chtourou, R. Enhancement of the photoluminescence

 doi:10.20944/preprints202407.1799.v1

property of hybrid structures using single-walled carbon nanotubes/pyramidal porous silicon surface. *J. Alloys Compd.* 2018, *731*, 978–984.
21. Rakita, Y.; Kedem, N.; Gupta, S.; Sadhanala, A.; Kalchenko, V.; Böhm, M.L.; Kulbak, M.; Friend, R.H.; Cahen, D.; Hodes, G. Low-Temperature Solution-Grown $CsPbBr_3$ Single Crystals and Their Characterization. *Cryst. Growth Des.* 2016, *16*, 5717–5725.
22. Lee, C.W.; Kim, J.G.; Gong, M.S. Humidity-Sensitive Properties of Self-Assembled Polyelectrolyte System. *Macromol. Res.* 2005, *13*, 265–272.
23. Arya, S.K.; Datta, M.; Singh, S.P.; Malhotra, B.D. Biosensor for total cholesterol estimation using N-(2-aminoethyl)-3-aminopropyltrimethoxysilane self-assembled monolayer. *Anal. Bioanal. Chem.* 2007, *389*, 2235–2242.
24. Zhang, M.; Tian, Z.Q.; Zhu, D.L.; He, H.; Guo, S.W.; Chen, Z.L.; Pang, D.W. Stable $CsPbBr_3$ perovskite quantum dots with high fluorescence quantum yields. *New J. Chem.* 2018, *42*, 9496–9500.
25. González-Pedro, V.; Veldhuis, S.A.; Begum, R.; Bañuls, M.J.; Bruno, A.; Mathews, N.; Mhaisalkar, S.; Maquieira, Á. Recovery of Shallow Charge-Trapping Defects in $CsPbX_3$ Nanocrystals through Specific Binding and Encapsulation with Amino-Functionalized Silanes. *ACS Energy Lett.* 2018, *3*, 1409–1414.
26. Saengdee, P.; Chaisriratanakul, W.; Bunjongpru, W.; Sripumkhai, W.; Srisuwan, A.; Jeamsaksiri, W.; Hruanun, C.; Poyai, A.; Promptmas, C. Surface modification of silicon dioxide, silicon nitride and titanium oxynitride for lactate dehydrogenase immobilization. *Biosens. Bioelectron.* 2015, *67*, 134–138.
27. Gunda, N.S.K.; Singh, M.; Norman, L.; Kaur, K.; Mitra, S.K. Optimization and characterization of biomolecule immobilization on silicon substrates using (3-aminopropyl)triethoxysilane (APTES) and glutaraldehyde linker. *Appl. Surf. Sci.* 2014, *305*, 522–530.
28. Peña-Alonso, R.; Rubio, F.; Rubio, J.; Oteo, J.L. Study of the hydrolysis and condensation of γ-Aminopropyltriethoxysilane by FT-IR spectroscopy. *J. Mater. Sci.* 2007, *42*, 595–603.
29. Ray, A.; Maggioni, D.; Baranov, D.; Dang, Z.; Prato, M.; Akkerman, Q.A.; Goldoni, L.; Caneva, E.; Manna, L.; Abdelhady, A.L. Green-Emitting Powders of Zero-Dimensional Cs_4PbBr_6: Delineating the Intricacies of the Synthesis and the Origin of Photoluminescence. *Chem. Mater.* 2019, *31*, 7761–7769.
30. Arshadi, S.; Moghaddam, J.; Eskandarian, M. LaMer diagram approach to study the nucleation and growth of Cu_2O nanoparticles using supersaturation theory. *Korean J. Chem. Eng.* 2014, *31*, 2020–2026.
31. Polte, Fundamental growth principles of colloidal metal nanoparticles – a new perspective. *J. CrystEngComm* 2015, *17*, 6809–6830.
32. Yin, Y.; Alivisatos, A.P. Colloidal nanocrystal synthesis and the organic–inorganic interface. *Nature* 2005, *437*, 664–670.
33. Akkerman, Q.A.; Motti, S.G.; Srimath Kandada, A.R.; Mosconi, E.; D'Innocenzo, V.; Bertoni, G.; Marras, S.; Kamino, B.A.; Miranda, L.; De Angelis, F.; Petrozza, A.; Prato, M.; Manna, L. Solution Synthesis Approach to Colloidal Cesium Lead Halide Perovskite Nanoplatelets with Monolayer-Level Thickness Control. *J. Am. Chem. Soc.* 2016, *138*, 1010–1016.